Optical and electrical properties of boron doped diamond thin conductive films deposited on fused silica glass substrates

M. Ficek[1], M. Sobaszek[1], M. Gnyba[1], J. Ryl[2], Ł. Gołuński[1], M. Smietana[3], J. Jasiński[3], P. Caban[4], and R. Bogdanowicz[1,5*]

[1] Department of Metrology and Optoelectronics, Gdansk University of Technology, 11/12 G. Narutowicza St., 80 233 Gdansk, Poland

[2] Department of Electrochemistry, Corrosion and Material Engineering, Gdansk University of Technology, 11/12 Narutowicza St., 80-233 Gdansk, Poland

[3] Institute of Microelectronics and Optoelectronics, Warsaw University of Technology, 75 Koszykowa St., 00-662 Warsaw, Poland

[4] Institute of Electronic Materials Technology, 133 Wolczynska St., 01-919 Warsaw, Poland

[5] Materials and Process Simulation Center, California Institute of Technology, Pasadena, California 91125, USA

Abstract. This paper presents boron-doped diamond (BDD) film as a conductive coating for optical and electronic purposes. Seeding and growth processes of thin diamond films on fused silica have been investigated. Growth processes of thin diamond films on fused silica were investigated at various boron doping level and methane admixture. Two step pre-treatment procedure of fused silica substrate was applied to achieve high seeding density. First, the substrates undergo the hydrogen plasma treatment then spin-coating seeding using a dispersion consisting of detonation nanodiamond in dimethyl sulfoxide with polyvinyl alcohol was applied. Such an approach results in seeding density of 2×10^{10} cm^{-2}. The scanning electron microscopy images showed homogenous, continuous and polycrystalline surface morphology with minimal grain size of 200 nm for highly boron doped films. The sp^3/sp^2 ratio was calculated using Raman spectra deconvolution method. A high refractive index (range of 2.0-2.4 @550 nm) was achieved for BDD films deposited at 500 ºC. The values of k were below 0.1 at λ=550 nm, indicating low absorption of the film. The fabricated

*Corresponding author: E-mail: rbogdan@eti.pg.gda.pl (Robert Bogdanowicz); Tel.: +48-58-347-15-03; Fax: +48 58-347-18-48

BDD thin films displayed resistivity below 48 Ohm cm and transmittance over 60% in the visible wavelength range.

1. Introduction

Diamond films have outstanding physical properties: mechanical, electrochemical, electronic, thermal and biological. Optically diamond is transparent from the ultraviolet, visible to far infrared region, resulting in many possible technological applications including optical coatings [1,2], optoelectronic switching devices [3], wide-band IR optical windows or high temperature and chemical corrosive operations [4]. Diamond is a wide bandgap semiconductor with E_g = 5.45 eV but when doped with boron its becomes *p*-type semiconducting material with outstanding electrochemical properties [5,6]. Boron-doped diamond (BDD) films are a great electrode material that have a wide electrochemical window from -1.25 to +2.3 V in aqueous electrolytes compared to standard hydrogen electrode (SHE) [7,8], high anodic stability [9], chemical stability in harsh environments [10,11], and biocompatibility [12,13]. These remarkable properties make BDD useful for many applications *e.g.* electrochemical sensing [14–16], biosensing [17,18], electrocatalysis [19–21], and wastewater treatment [22–24].

Chemical vapor deposition (CVD) technology allows for the production of high-quality diamond thin films. The two most common techniques to synthesise BDDs are hot-filament CVD (HF-CVD) [25] and microwave plasma-assisted CVD (MW PA CVD) *in-situ* doped with boron precursors [26]. The boron dopant density, achieved by using MW PA CVD, ranges from 10^{16} to 10^{21} atoms cm^{-3} and *p*-type semiconducting materials transform to semimetal for the dopant density at $2 \cdot 10^{20}$ [25]. The various applications require that structural and morphological properties be optimized: smoother surfaces, optical transparency or electrical conductivity. Growth parameters such as gas mixture, temperature, pressure and boron dopant density influence not only the morphology and structure (sp^3/sp^2 ratio) [27,28], but also electrical and electronic properties or optical transparency. Boron dopant density has significant influence on all of these properties which has been confirmed by literature. The average grain size on the diamond film decreases up to 10 times with increasing boron density and was investigated by Liao *el al.* [29]. Boron introduces re-nucleation which result in the creation of smaller crystalline on primary higher diamond crystals. Recently, Lu *et al.* [30] has shown a direct visualization of boron dopant distribution and has concluded that boron dopants clearly demonstrate the presence in the diamond lattice and an enrichment of these dopants within twin boundaries and defect centres.

2

Several papers report optical properties of BDD films deposited on silicon substrates. Gupta *et al.* [31–33] applied spectroscopic ellipsometry (SE) to investigate BDD films with varying boron density. Hu *el al.* [34] and Gupta *et al.* [33] show ellipsometric angles Ψ, Δ and dielectric constants in a range of 200 up to 1230 nm (1.0 ÷ 5.5 eV). Zimmer *et al.* [35] investigated heavily boron-doped nanocrystalline diamond films using spectroscopic ellipsometry. NCD film was deposited on Si wafers at the mean dopant level [B]/[C] of 6500 ppm and with the complex index of refraction calculated from the Lorentz model in the VIS-NIR range (up to 950nm). Next, Gajewski *et al.* [36] investigated the optical parameters, namely, photocurrent and optical absorption coefficient in undoped and low-doped nanocrystalline diamond films deposited on monocrystalline silicon. The results of spectrally resolved photocurrent and photothermal deflection spectroscopy in the low energy range, between 0.5 and 1.0 eV, confirmed that boron as well as sp^2 carbon phases in the grain boundaries govern the optical-absorption process.

A few reports can be found that focus on boron doped diamond optical transparent electrodes. Stotter *et al.* [37,38] enhanced boron doped diamonds electrodes to spectroelectrochemistry studies in the UV wavelength region showing good transparency at 50 – 60%. Mermoux *et al.* [39] used confocal Raman imaging to study OTEs for samples with a thickness of 380 μm. Remes *et al.* [40] investigated the optical properties of undoped NCD film on fused silica by using photothermal deflection spectroscopy, calorimetry and dual beam photocurrent spectroscopy. Kromka *et al.* [41] investigated the impact of low-temperature MW CVD process on optical properties of nanocrystalline diamond films (NCD) on silicon and quartz substrates; the films displayed a transmittance of ca. 70% and a high refractive index of 2.34 at 550 nm of wavelength. Potocky *et al.* [42] showed a refractive index of 2.2 to 2.4 (@550 nm) on quartz substrate for growth temperature below 400 °C. The optical properties of diamond layers strongly depend on deposition temperature [43,44]. In addition, various boron doping has a crucial impact not only on electronic properties but also on optical properties. A boron dopant introduces an acceptor level located at 0.38 eV from the top of the valence band [45,46] shifting both absorption edge and refractive index.

In our previous works we reported seeding in different suspensions (water / DMSO) for obtaining diamond films [47] or growth of BDD on fused silica [MMS] but only for one doping level. Scorsone *et al.* proposed seeding in a solution composed of polyvinyl alcohol (PVA) and detonation nanodiamond (DND) particles but it was studied just on Si wafers. PVA was chosen due to its ability to form thin films as well as its high viscosity and high solubility in water and surfactants [48,49].

To the best of our knowledge, there is still a lack of information about optical and electronic properties of boron-doped diamond deposited on fused silica substrates and their boron concentration dependence. These parameters are critical for developing the integrated optical sensors [50,51], transparent electronics [52] and optoelectrochemical biosensing devices [53,54].

In the present study we applied a novel two step seeding process of fused silica substrates to achieve high seeding density and BDD film homogeneity. First, we used pre-treatment of fused silica substrates in hydrogen plasma. Then, substrates were seeded by spin-coating with PVA mixed with diamond slurry, the latter based on diethyl sulfoxide (DMSO) and diamond nanoparticles. The main novelty of the paper is the study of optical and electrical properties of undoped and boron-doped ($[B]/[C]_{ppm}$ ratio between 1000 and 10000) diamond films in two molar ratios of CH_4-H_2 mixture (1% and 4%). Our motivation to present this investigation has been derived from the optimization growth parameters process of the chemical vapour deposition to achieve BDD film with enhanced optical and electrical properties for the purposes of fibre optical coating and opto-electro active electrode for energy conversion, optical sensors and spectroelectrochemistry. Thin boron-doped films were deposited by MW PA CVD method on fused silica substrates. Micro-Raman spectroscopy was used to examine molecular structure of the BDD films (sp^3/sp^2 band ratio). Optical properties, thickness and roughness in VIS-NIR wavelength range were investigated by means of *ex situ* spectroscopic ellipsometry (SE). Moreover, the optical band-gap energy E_g was obtained using Tauc's plot. Electrical properties were investigated 4-point probe method.

2. Experimental

2. 1. Fused silica glass pre-treatment

The mirror polished fused silica glass slides were used as a substrate for experiments (10x10 mm; 1 mm thick). Before treatment, the quartz slides were cleaned for 5 minutes in an ultrasonic bath containing acetone, rinsed in 2-isopropanol and then dried.

The substrates then undergo the hydrogenation in the plasma. The process was performed in microwave H_2 plasma at 1300W for 60 min. During the process the total flow of gas reached 300 sccm and the pressure was kept at a level of 50 Torr. Hydrogenation was supposed to change surface termination and wetting properties, which decrease seeding density of diamond thin films. The seeding process included spinning of thin film of DND

4

seeding media by use of spin-coater (Laurell WS-400B, USA). The home-made DMSO-PVA-DND suspension with nanodiamond concentration of 0.25% w/w in DMSO/PVA were used in experiments. The DND slurry preparation procedure has been reported elsewhere [55].

2. 2. CVD diamond deposition on fused silica glass

The BDD electrodes were synthetized in an MW PA CVD system (SEKI Technotron AX5400S). Substrate temperature was kept at 500°C during the deposition process. Highly excited plasma was ignited by microwave radiation (2.45 GHz) [56,57]. The plasma microwave power, optimized for diamond synthesis, was kept at 1300 W. The molar ratio of CH_4-H_2 mixture was kept in this study at 1% and 4% of gas volume at 300 sccm of total flow rate. The base pressure was about 10^{-6} Torr and the process pressure was kept at 50 Torr. The doping level of boron in the gas phase, expressed as [B]/[C] ratio, was 0, 1000, 2500, 5000 and 10 000 ppm using diborane (B_2H_6) dopant precursor. The growth time was 60 minutes, producing polycrystalline films with thickness from 300 to 700 nm. All the different parameters of deposition for each sample are listed in Table 1.

Table 1. A set of samples and the corresponding deposition parameters.

Sample	CH_4 [%]	[B]/[C] ratio [ppm]	T_c [°C]
Q_1_0	1	0	500
Q_1_1	1	1000	500
Q_1_2.5	1	2500	500
Q_1_5	1	5000	500
Q_1_10	1	10000	500
Q_4_0	4	0	500
Q_4_1	4	1000	500
Q_4_2.5	4	2500	500
Q_4_5	4	5000	500
Q_4_10	4	10000	500

2. 3. Analytical methods

The water contact angles were measured by the sessile drop method (drop volume ~0.5 μl) using a home-made contact angle meter equipped in B/W high resolution CDD camera.

5

The determination of the angle between the solid surface and the tangent of the drop was performed by computer control. Three measurements were performed on each surface, and arithmetic means and standard deviations were calculated by using Origin 6.1 software package (OriginLab Corp., Northampton, USA).

A scanning electron microscope (S-3400N, Hitachi, Japan) with a tungsten source and variable chamber pressure (VP-SEM) was utilized to inspect the surface of synthesized thin films. The surface topography was examined with an atomic force microscope (AFM) (Veeco Nanoman V, Veeco Instruments Inc., New York, NY, USA) in tapping mode. The imaging tapping mode and standard Si tips were used to perform the surface characterization. The scan size was 2 μm × 2 μm.

The molecular composition of the films was studied by means of Raman spectroscopy using Raman confocal microscope (Horiba LabRAM ARAMIS, Japan). Spectra were recorded in a range of 200–3500 cm^{-1} with an integration time of 2 s, using a 532 nm diode pumped solid state (DPSS) laser in combination with a 100x objective magnification (NA = 0.95) and 50 μm confocal aperture. The relative sp^3/sp^2 band ratios were determined by deconvolution of Raman spectra with use of Gramms/AI Suite (ThermoScientific, USA) and comparison of integral intensity of a band assigned to diamond (approx. 1332 cm^{-1}) and a wide "G" band assigned to distorted sp^2 phase (between 1520 and 1600 cm^{-1}).

Spectroscopic ellipsometry investigations were carried out with a phase-modulated ellipsometer Jobin-Yvon UVISEL (HORIBA Jobin-Yvon Inc., Edison, USA). The investigated wavelength region was 250–800 nm with a step of less than 0.5 nm. The experiments were carried out at room temperature using an angle of incidence fixed at 60° and the compensator was set at 45°. The incidence angle resulted from Brewster's angle of quartz glass substrate. DeltaPsi software (v. 2.4.3) was employed to determine the spectral distributions of refractive index n (λ) and the extinction coefficient k (λ) of the diamond films.

The BDD deposited on fused silica were studied by 4-point probe for electrical characterization. Prior to the measurements, the Ohmic contacts (Ti/Au) were deposited on the BDD samples. The room temperature resistivities were measured by four-point probe placed in a straight line with equal interprobe spacing (s = 1.5 mm). The needle-like probes with a radius of 100 μm were utilized. The size of samples was 1 x 1cm. The correction factor of 0.86 was taken into account during resistivity estimation due the finite sample size [58,59]. A source meter (Keithley 2400, UK) was used as a current source applied to the external probes. The current was gradually increased from 0 up to 100μA with a step of 1μA. Voltage

6

on the internal probes was measured with a VA multimeter (Appa 207, Taiwan). Each sample was measured 10 times at four various surface points and averaged resistivity was presented.

3. Discussion and results

3. 1. Surface properties and film composition

The PVA-DMSO-DND slurry contact angle measurements were investigated to study the influence of hydrogenation on the surface wetting of fused glass substrates. Water-based wetting studies has been presented as the reference. The hydrogen modification of fused silica glass with microwave plasma treatment leads to strongly changed contact angles in comparison to the bare glass surfaces (see Figure 1).
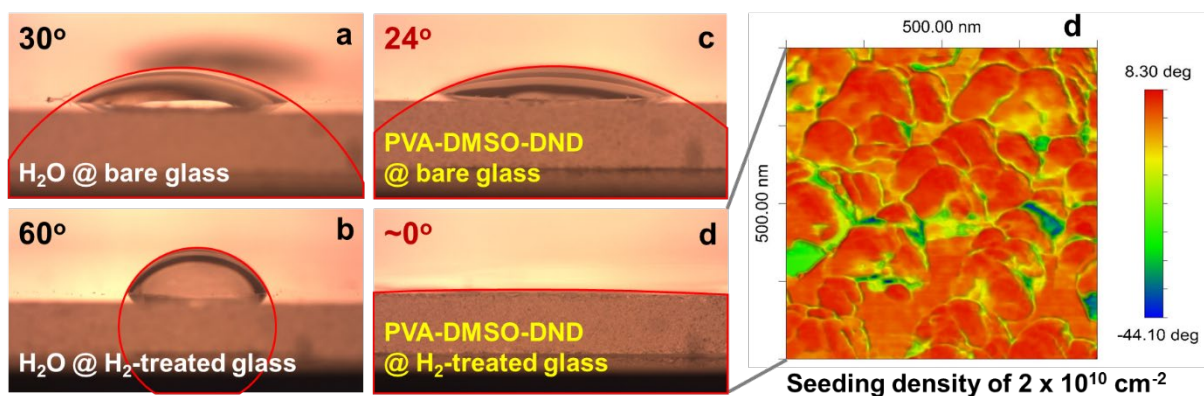

Figure 1. Wetting properties of fused silica substrate before and after hydrogenation treatment.

Both the H_2O and the PVA-based DND slurry results in a similar level of contact angles recorded at bare, untreated fused silica substrates ($\theta \sim 30 \pm 2°$). However, the hydrogenation of fused silica induces increase of contact angle up to $\theta = 60 \pm 2°$ in case of H_2O wetting. This increase of hydrophobicity is attributed to hydrogen termination of the surface inducing charge [60] and surface energy shift [61].

In case of PVA-based slurry wetting, we have observed quite the opposite effect. The hydrogen treatment provides enhanced wetting of substrate and considerably smaller contact angles with values close to $\theta = 0 \pm 2°$. The mechanism is supposed to be the same as before. The bare fused silica substrates are predominantly terminated by oxygen or hydroxyl groups. Such substrates exhibit semi-hydrophilic character mainly due to the negative surface charge. The hydrogenation of fused silica introduces partial hydrogen termination inducing a considerable shift towards positive charges.

The polyvinyl alcohol is known to form aggregates with round the surface of nanoparticles contributing towards the negative charge behaviour [62]. Thus, the negatively charged PVA-based DND slurry shows enhanced wetting and adsorption due to electrostatic interactions with positively charged hydrogen treated fused silica. Finally, enhanced wetting of the surface by PVA-DMSO-DND slurry produces relatively high seeding of 2×10^{10} cm^{-1} as measured by AFM image estimation and illustrated in Figure 1D.

The laser Raman spectroscopy is a powerful technique for characterizing the distinctive energies of the chemical bonds or for distinguishing between different phases of the same material, such as diamond or graphite. Raman spectra of boron-doped diamond films with different boron and methane concentration in the process gas mixture has been illustrated in Figure 2.

The intensity bands in the Raman spectra of deposited BDD films attributable to diamond lattice at 1318–1333 cm^{-1}, and nanocrystalline diamond at 1126–1136 cm^{-1} were registered in heavily doped-diamond films. Moreover, the differences in boron content in samples can be confirmed by the growth of the band at 1231 cm^{-1} and a decrease in signal intensity above 1650 cm^{-1}, which is typical for a highly boron doped CVD diamond [63]. The line near 1220 cm^{-1} is likely to be caused by the effect of boron on the diamond lattice, and its appearance in the spectrum is independent from the presence of the sp^2 carbon phase in the films. This finding is supported by the results obtained in [64], where boron-doped homoepitaxial diamond was studied, and in [65], where diamond, synthesized at high pressures and temperatures was studied. Moreover, the authors of [66] performed *ab initio* calculations of the properties of the diamond lattice in which some of the carbon atoms were replaced by boron atoms and showed that apart from a maximum at 1289 cm^{-1} (which is close to the diamond line at 1333 cm^{-1}). The D band at 1346 cm^{-1} can be assigned to the mixture of amorphous sp^2 and sp^3 carbon, while the G band at 1556–1558 cm^{-1}, to sp^2 amorphous carbon.
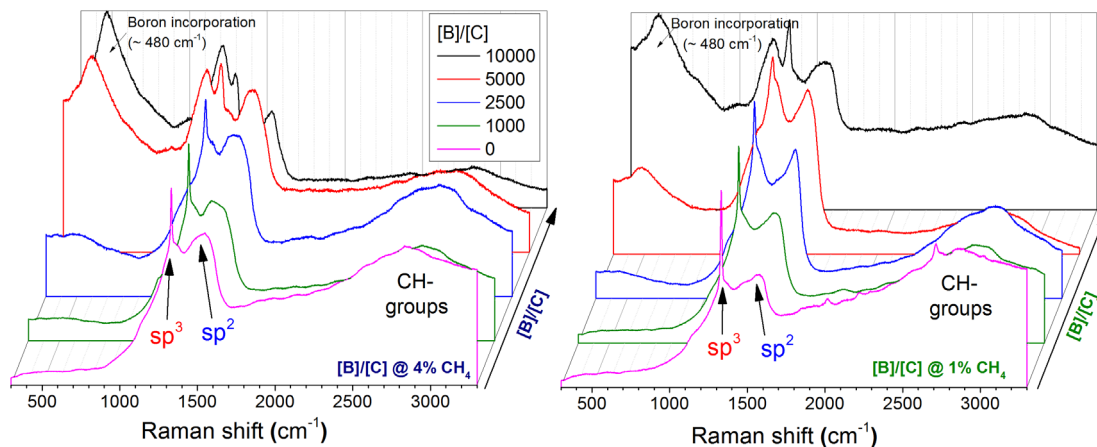
Figure 2. Raman spectra of boron-doped diamond films ([B]/[C]=0; 1000; 2,500; 5000; 10000 ppm) deposited at fused silica in temperature of 500°C vs. two different methane concentrations (1% and 4%) in gas mixture.

The authors of [67] calculated that for [B]/[C] ratio of [B]/[C]=2000 and 20,000 ppm, the shifts of the Raman scattering peak of diamond films relative to natural diamond peak at 1332 cm^{-1} were about 0.5 and 3.6 cm^{-1} that correspond to a tensile residual stress of 0.2 and 1.2 GPa, respectively. This increase of residual stress agrees with the results observed by Wang *et al.* [68], which were attributed to impurities band formed when a metallic like conductivity character of doped films is observed, in the most times, at boron concentration of around 10^{21} cm^{-3}. It is important to remember that even heavily doped films with boron concentration up to 10^{20} cm^{-3} have shown good quality and crystallinity verified by Raman spectroscopy and SEM morphology.

As the boron concentration increases, the intensity of the line at 1231 cm^{-1} grows in respect to the diamond line, which was shown to decrease and shift toward low frequencies. This inversely proportional dependence of the line intensities is assumed to be associated with an increase in the number of cells in which a boron atom substitutes for a carbon atom (i.e. with a decrease in the number of purely diamond cells). The larger electron shell radius of boron results in an increase in the lattice parameter [69,70] and a 5% [66] decrease in the elastic constant as compared to that of the C–C bond. These factors explain the shift in the diamond line toward low frequencies. A similar shift in Raman lines was observed not only in doped diamond but also in other structures, such as amorphous carbon nitride [71].

This finding has been confirmed by a significant decrease in the band assigned to diamond and low *sp³/sp²* band ratio listed in Table 2. The full width at half maximum (FWHM) of

9

diamond band was in the range that is typical for CVD diamond (10-12 cm^{-1}) for low doped diamond samples (see Table 2). As [B]/[C] ratio increases, the FWHM of diamond band get broadened up to ca. 40 cm^{-1} or 70 cm^{-1} for 1 and 4% CH$_4$ grown samples respectively. Since the diamond structure became more distorted, the relative sp^3/sp^2 band ratio of diamond films decreased as listed in Table 2.

The shifting of the Raman bands assigned to diamond and the changes of bandwidth (FWHM) are attributed to local stresses at film/fused silica interface, which results from non-epitaxial deposition of diamond on an amorphous substrate and non-homogeneous boron doping incorporation creating sp^2 rich clusters. These findings are in agreement with sp^3/sp^2 band ratio trend and with previous works [23] reporting BDD growth at monocrystalline Si wafers. It is worth noting that the diamond structure is much more affected by [B]/[C] or % of CH$_4$ when films are deposited on fused silica than crystalline materials i.e. Si, metals.

Table 2. The ratio of sp^3/sp^2 Raman bands, and the FWHM of the Raman band (1332 cm^{-1}) estimated for BDD samples deposited on fused silica.

Sample	sp^3/sp^2 (rel.)	sp^3 peak position (cm^{-1})	FWHM (cm^{-1})
Q_1_0	0.471	1331.2	10.7
Q_1_1	0.397	1332.4	12.3
Q_1_2.5	0.233	1324.3	13.6
Q_1_5	0.164	1322.9	28.9*
Q_1_10	0.173	1319.4	37.8*
Q_4_0	0.249	1331.2	12.2
Q_4_1	0.173	1331.2	16.3
Q_4_2.5	0.096	1328.8	26.4
Q_4_5	0.071	1314.6	56.6*
Q_4_10	0.050	1300.4	68.2*

* the uncertain values due to peak interferences and Fano effect.

The surface analysis of boron-doped diamond films, taken by SEM (see inset Figure 3), showed a variation of surface morphology as a function of doping. An average grain size of 0.5–1 µm was obtained at low doping levels but the grain size decreased as the doping level increased, reaching values of approx. 200 nm. Miryata *et al.* [72] and Cifre *et al.* [73]

reported analogous results, attributed to the boron effect, which enhanced the nucleus formation during the first step of growth. Consequently, higher doping levels promote a smaller grain size, lower growth rate and lower roughness as compared with the values obtained using low doping levels [29,68,74].

The growth rate g_{rate} of BDD films was investigated independently by spectroscopic ellipsometry and stylus profilometer and averaged. The deviation of thicknesses obtained by both methods was not higher than 20%. Figure 3 illustrates the variations in average growth rates versus [B]/[C] gas phase and methane admixture. The influence of methane admixture is known and obvious [75,76]. The increase of CH_4 flow from 1% up to 4% doubled the g_{rate} of all BDD films achieving values of approx. 4 nm min^{-1} and 8 nm min^{-1} respectively. A comparable growth rate has already been reported for fused silica [42]. Independently on the methane admixture, the increase of boron doping level first enhances kinetics of the diamond growth (up to [B]/[C] 1000 ppm). The primer increase of g_{rate} is followed by slowing and saturation of BDD growth. The higher boron incorporation impairs growth kinetics mainly due to the more intensive distortion of the diamond lattice and synthesis of non-diamond form rich in boron pairs and sp^2 hybridised allotropes [77]. Moreover, the values of surface roughness (SRL) of BDDs are also presented in Figure 3. The ellipsometrically estimated SRL are significantly smaller than film thicknesses or crystallites size, keeping the values below 50 ± 5 nm. The most reasonable explanation for the observed phenomena is the heteroepitaxial diamond nucleation and growth. The characteristic columnar films structure exhibits various planar crystallite size with relatively flat surface , predominantly composed of {100} and {111} faces when grown on a non-diamond substrates [78].
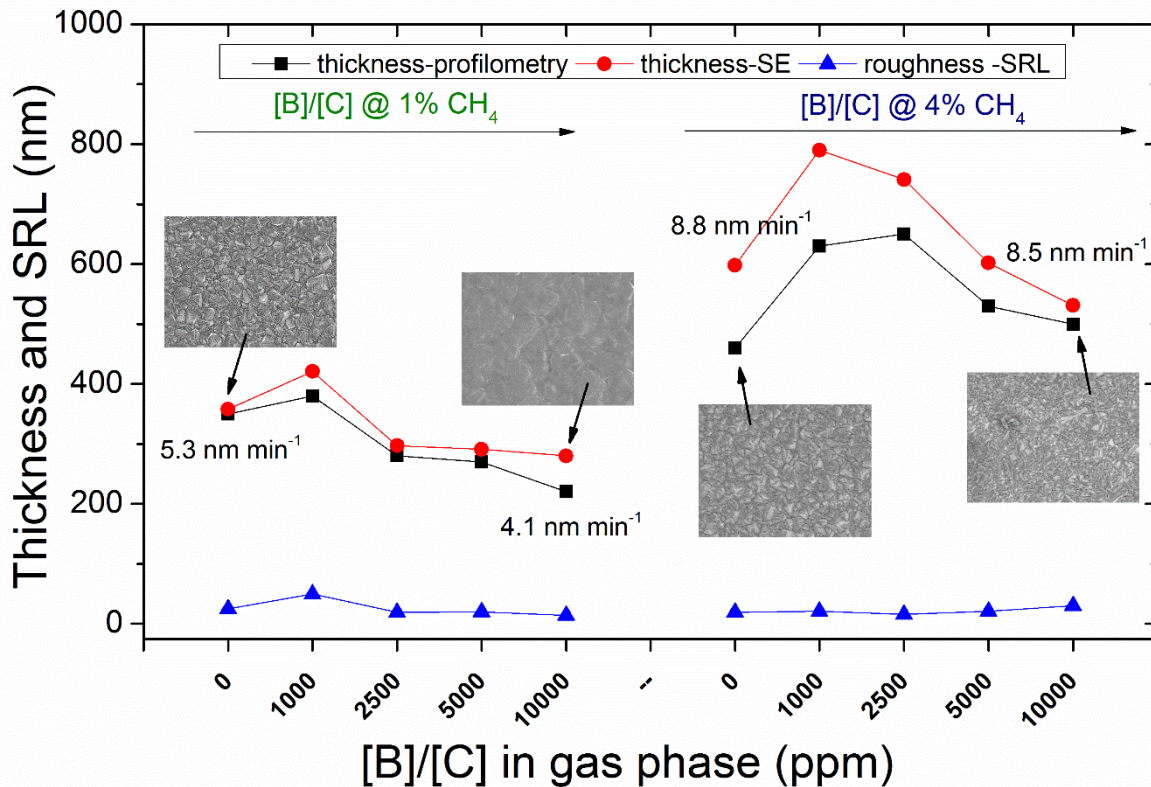
Figure 3. Thickness and surface roughness (SRL) of the BDD samples deposited on the fused silica estimated by stylus profilometer and spectroscopic ellipsometry. Growth rates of BDD films are placed in plot for comparison of time kinetics. Insets: SEM micro-images of BDD surface (3 x 2 μm) taken with magnification of 10 000 x.

3. 2. Optical properties

The ellipsometric parameters Ψ, Δ were measured for 70° angles of incidence in the wavelength from 260 nm to 830 nm at room temperature. A five-layer structural model (ambient/SRL-surface roughness layer/BDD/intermix/glass – substrate) was applied to the samples in order to determine the effective thickness of SRL, and the thickness of BDD film and its effective complex dielectric function $\langle \hat{\varepsilon} \rangle = \varepsilon_1 + i\varepsilon_2 = \langle \bar{n} \rangle^2$, where $\varepsilon_1, i\varepsilon_2$ and $\langle \bar{n} \rangle^2$ are the real part, the imaginary part of $\langle \hat{\varepsilon} \rangle$ and the effective complex refraction index, respectively. The top layer has a composition of the film with spaces filled with air. Such approach allowed for estimating the average roughness of the films. The thickness of intermix layer [79] had been derived in the previous investigation and was set as 2 nm for all samples in this study. The optical responses of roughness and intermix layers were estimated using Bruggeman effective medium approximation (EMA) [79,80]. The diamond film has been assumed to be an isotropic, homogeneous material and its dispersion was fitted to the Tauc-

12

Lorentz oscillator (TL) model. This model has been used recently for amorphous semiconductors by Gioti *et al.* [81,82]. TL model is also widely applied to model the dispersion of the optical properties of a-C, a-C: H [83] as well as diamond polycrystalline films [84]. The model is a combination of the Tauc joint density of states [81] and the quantum mechanical Lorentz oscillator model [82]. The TL model fits to the dielectric functions of a class of amorphous materials. The parameters of the TL model were fitted for each of the analysed films.

Finally, the assumed optical model was fitted to the experimental data using the non-linear Levenberg- Marquardt regression method and mean-square error of minimization (MSE) [85]. As a result of SE analysis, the thickness and optical constants, i.e. refractive index $n(\lambda)$ and extinction coefficient $k(\lambda)$ were obtained.
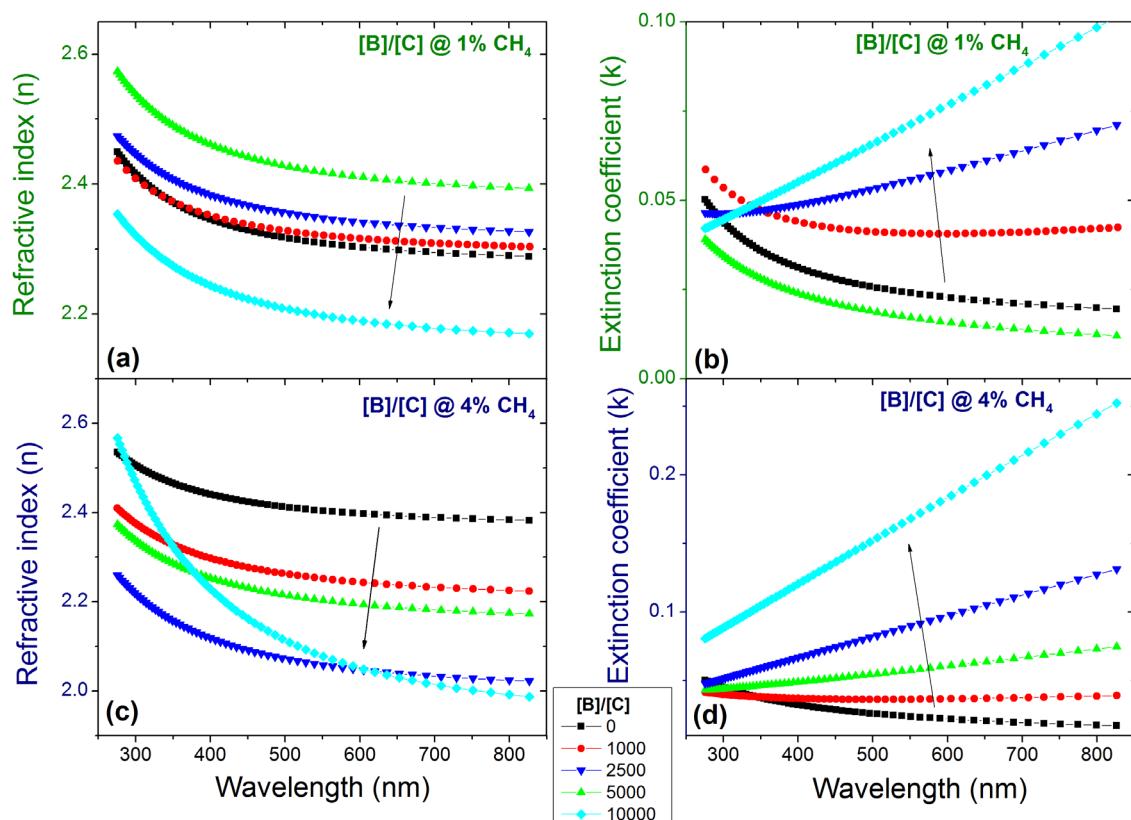

Figure 4. Variation of optical constant for boron-doped diamond films obtained on quartz slides at various boron doping level and methane admixture.

Spectral variation of $n(\lambda)$ and $k(\lambda)$ for diamond films deposited at 1% and 4% of methane versus different boron concentration in process gas phase at 500°C during a 60-min process are presented in Figure 4. All the deposited diamond films show normal dispersion of refractive index in studied wavelength range. The *n* decreases with increasing wavelength,

13

exhibiting a typical behavior near the band gap of electronic transition. Just in case of 4% CH_4, the n values of highly boron-doped diamonds are slightly shifted towards higher wavelengths in comparison to a single-crystal diamond (SCD) and other BDD samples.

The achieved values of n were high, ranging from 2.0 to 2.4 for BDD films deposited with low and medium boron doping level (Figure 4AC). Hu *et al.* [43,44] reported the values of n between 2.31 and 2.34 for NCD films, while Gupta *et al.* [86] determined the n values between 1.7 and 2.1 for microcrystalline diamond (MCD) films at λ= 632 nm. The n values, when compared to SCD, indicate lower physical and optical density of films [87,88]. In general, the refractive index decreases as the doping level increased (see Figure 4 and 6). The observed effect is attributed to boron incorporation in the BDD structure. A similar effect, namely a decrease in the film refractive index with increasing level on boron-doped diamond has also been observed for other carbon-based films obtained with plasma methods [76]. Most likely, the samples contain more C-H defects, boron pairs, sp^2 hybridized phases as revealed by Raman studies (see Figure 2). The increased boron doping level stimulates distortion of tetrahedral lattice.

The k values as illustrated in Figure 4BD were below 0.06 and 0.2 at 550 nm for 1% and 4% of methane admixture respectively. Boron doping with [B]/[C] below 5000 ppm results in extinction coefficient much below 0.05, indicating low light absorption over the BDD film. That parameter is critical for optical application of deposited BDD films. The highest level of boron doping, while showing low resistivity, cannot be applied in optical devices due to high k values. The highly boron doped films ([B]/[C] > 5000 ppm) exhibits abnormal character of extinction plot; higher values with increasing wavelength. Our pervious IR studies showed that the energy of the absorption line ranges to 0.29 eV, which is close to the boron acceptor level (0.38 eV) formed during the incorporation of the B atoms in the diamond lattice [89]. This effect was also discussed in [45,46,90]. This also means that the critical boron concentration needed for the metal-insulator transition was achieved for the produced highly boron doped films.

The estimated optical constants variation implies the transmittances of grown BDD films. Figure 5 presents intrinsic transmittance for BDD films in the wavelength range of 250 nm to 850 nm calculated using the determined optical constants and thickness. The transmittance of layers with low or medium [B]/[C] reaches over 60% in the VIS-IR range. Such transmittance values are sufficiently high with regard to a possible application of the films in optical sensing [91], while the highly boron doped films (i.e. Q_1_10) reveal a critical decrease in transmittance to ca. 40% when compared to other grown samples. The effect is even more

14

pronounced (i.e. Q_4_10) in the case of 4% of CH_4 admixture than for BDD grown with 1% methane addition.
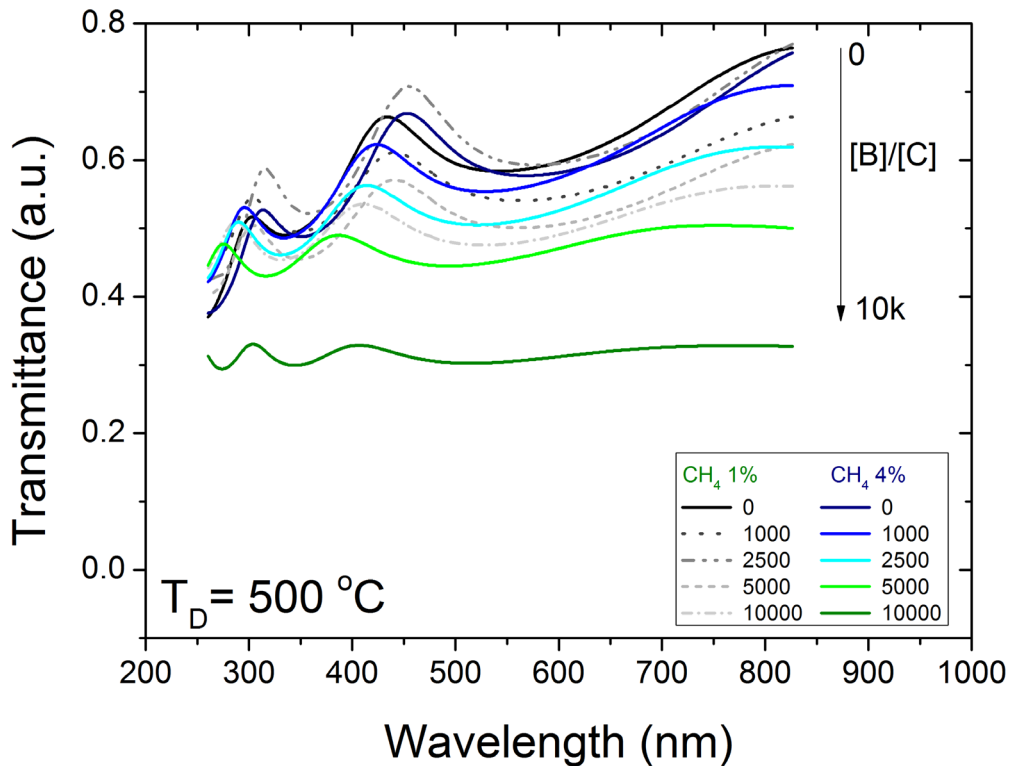

Figure 5. Transmittance of BDD films deposited at fused silica substrates vs various boron doping and methane admixture.

The transmittance values correspond directly with the molecular structure – sp^3/sp^2 (see Figure 2 and Table 2). The Q_4_10 sample was very opaque, with the transmittance of about 30%. This characteristics was caused by an abundance of the sp^2 like "cauliflower" [92] structure during the early stage of film growth. Next, it can be noticed that the transmittance decreases with both the concentration of boron during diamond growth and methane admixture increasing. It is also worth noting that Figure 5 shows transmittances of BDD films with various thicknesses resulting from different g_{rate} values. While the Q_1_X samples achieves average thickness half smaller than Q_4_X ones, they finally result in a similar or slightly higher transmittance level. If the growth time will be optimized to produce films with similar thickness, the higher transmittances will be obtained for 4% of CH_4, mostly due to the smoother surface and smaller crystallites size limiting the light scattering effects.

The comparison of refractive index at 550 nm and optical band gap values for different boron-doped levels in diamond and two different methane concentration in gas mixture are

15

shown in Figure 6. The optical band gap E_{gopt} was determined from the absorption coefficient α by using a Tauc plot [93]. The Tauc plot analysis indicates that band-to-band indirect transitions are more probable than direct transitions. Therefore, the band gap values were estimated by extrapolating the linear portion of the $(\alpha h\nu)^{1/2}$ vs. $h\nu$ plot, where $h\nu$ is the photon energy, to $(\alpha h\nu)^{1/2}=0$. This assumption is supported by other reports delivered by Lee *et al.* [94], Hu *et al.* [34] or Taylor *et al.* [95].
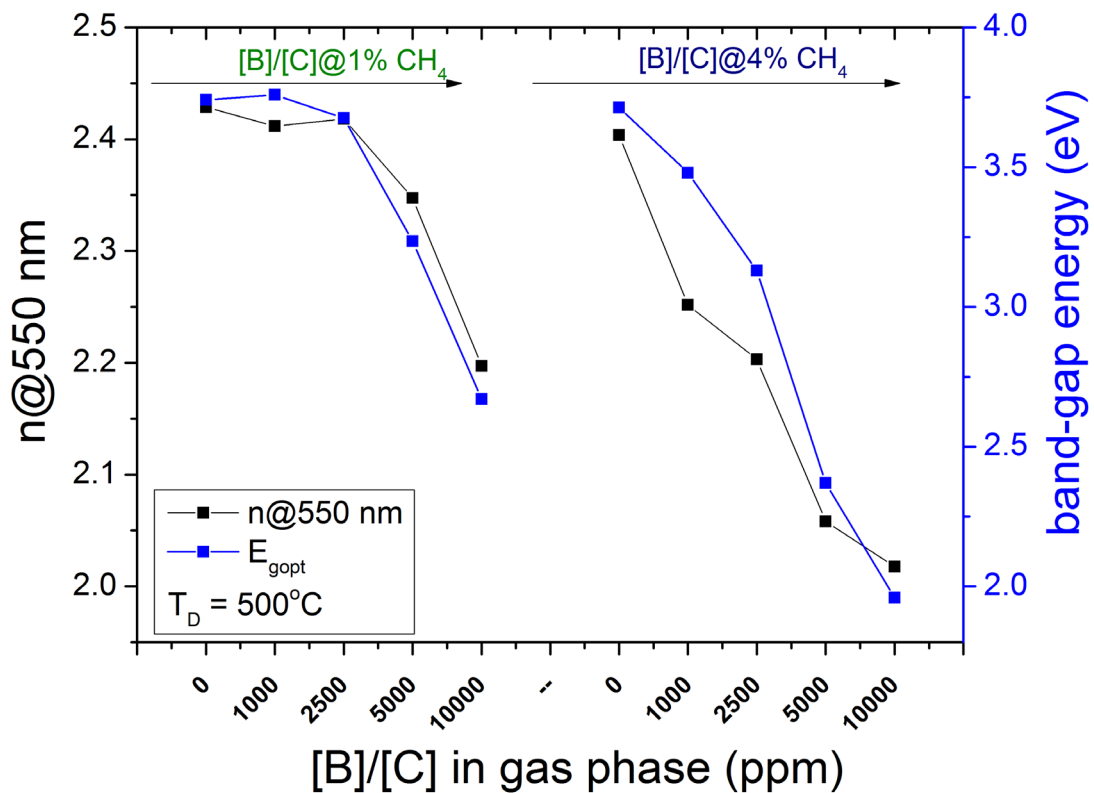

Figure 6. Refractive index recorded at 550 nm and in-direct optical band gaps of BDD samples with increasing boron concentrations and various methane admixture.

Both estimated parameters decrease with increasing boron doping level. The E_{gopt} trend was compared with the refractive index changes to show the agreement of Tauc estimation. Furthermore, the higher methane admixture (Q_4_X) pronounces this influence and makes the trend more radical. The gap E_{gopt} significantly decreases from 3.7 eV estimated at [B]/[C] of 0 ppm sample down to 2.15 eV and 2 eV achieved for the Q_1_10 and the Q_4_10 films respectively. The obtained values of the optical band gap are reasonably small compared to that achieved previously by Sobaszek et al. [89] or by Hu et al. [34] with Si wafers. Nevertheless, the gap estimated here E_{gopt} values are close to that presented for heavily boron-doped NCD films by Zimmer *et al.* [35] or for B-NCD by Taylor *et al.* [95]

16

grown with monocrystalline silicon. The variation of optical band gap correlates directly with the higher refractive index, accordingly the similar phenomena stands behind its changes.

3. 3. Resistivity investigation of BDD films

The four-point probe method was used to measure the resistivity of BDD films deposited on fused silica. The reference samples of BDD films deposited at thick silicon oxide have been shown and discussed for comparison. While the film thickness was much smaller than the distance between the probes, the surface resistivity was calculated from formula (1):

$$R_{sh} = \frac{\pi}{\ln(2)} \cdot \frac{V}{I} \cdot h \cdot f_2 \qquad (1),$$

where V is the voltage measured at the internal probes, I is the current value applied to the external probes, h is the film thickness and f_2 is the correction factor [58,59].

Figure 7 illustrates the surface resistivity dependence of boron doped-diamond films in function [B]/[C] ratio, which was determined by studies of 4-point probe followed by estimation by equation (1).

It is evident that a higher [B]/[C] level leads to a decrease of BDD film resistivity. However, this trend shows non-linear character. The primary reduction of resistivity versus [B]/[C] ratio is followed by its saturation or just slight decrease. This non-linear trend in resistivity is known as the border between metallic and hopping conduction [96]. In case of BDD deposited at fused silica, it was observed that with the increase of [B]/[C] concentration in gas phase from 0 ppm to 2500 ppm, the film resistivity significantly drops from 4 kΩ cm to value of 48 Ω cm and then there is a slight decrease in film resistivity to 35 Ω cm and 15 Ω cm for samples with [B]/[C] ratio of 5000 and 10,000 ppm respectively. The methane admixture has also influence of the film resistivity of highly boron-doped samples (Q_X_5, Q_X_10) causing a shift from 35 Ω cm and 15 Ω cm down to 18 Ω cm and 10 Ω cm, when changed from 1% to 4%.
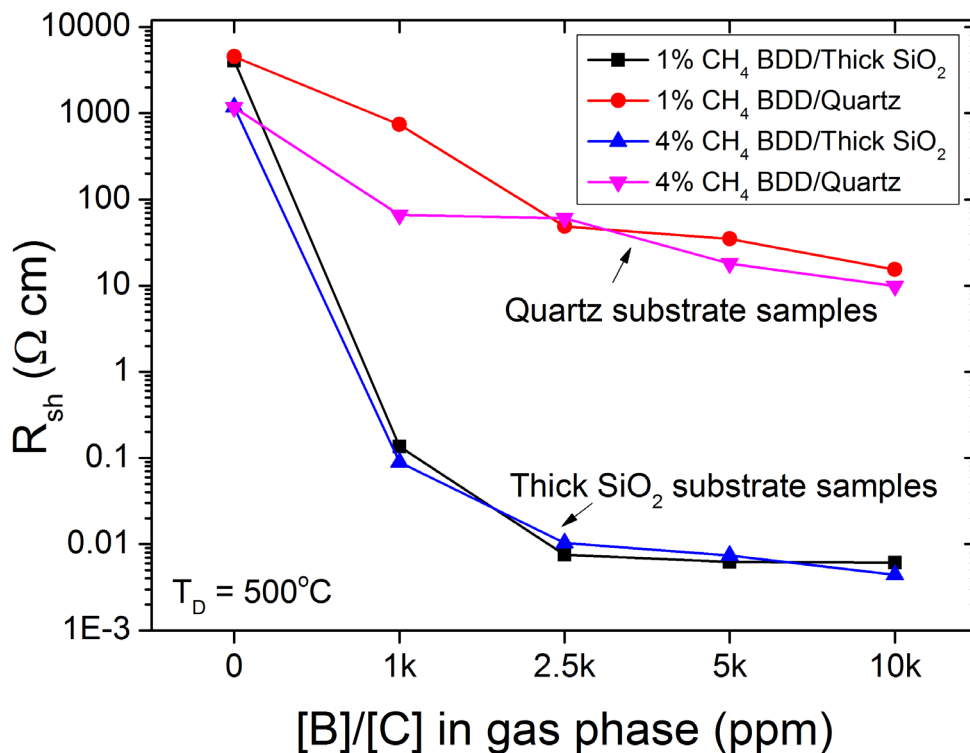
Figure 7. Surface resistivity of BDD films vs various boron doping level and methane admixture in the plasma. The BDDs deposited on fused silica and silicon wafer covered by thick SiO_2 have been presented for comparison.

It is worth noting that the reference BDD samples result in a reasonably small resistivity comparing to fused silica grown ones, but both trends are in direct agreement. The BDD surface resistivity recorded at thick oxide substrates reaches approximated values of 100, 10 and 5 mΩ cm for 1,000; 5,000 and 10,000 ppm of [B]/[C] respectively. The authors attribute this effect to differences in structure of both substrates influencing distortion of diamond lattice (i.e. smaller crystallites size, decreased thickness, and higher sp^2 content or impurity states in band gap) [97]. Unlike its related thick SiO_2 crystalline phase, fused silica is amorphous material with a macroscopic inversion symmetry that promotes growth of non-diamond phases. Besides, it could be easier dehydrated by hydrogen rich plasma generating oxygen species [98,99] responsible for boron incorporation saturation [100]. Furthermore, the smaller resistivity might also be caused by charge tunnelling effect to the Si wafer substrate, which is driven by the impurities in thermally fabricated thick oxide films.

Summarizing, the surface resistivity of BDD films grown at fused silica are about one order higher than the values reported at monocrystalline Si wafers [101,102]. It is worth mentioning that the higher resistivity of fused silica based BDDs could be an effect of lower

18

thickness, diffusion of the carriers on the smaller grains or defects induced by amorphous structure of substrates. Moreover, Tsigkourakos *et al.* [103] reported that the undoped DND seeds lead to the presence of non-conductive areas at the diamond film – substrate interface, impacting strongly on the interfacial resistance which becomes proportional to the seed layer surface coverage. That effect is even pronounced by the PVA-based seeding procedure applied here, resulting in high density seeding process mainly due to PVA-DND clusters formation.
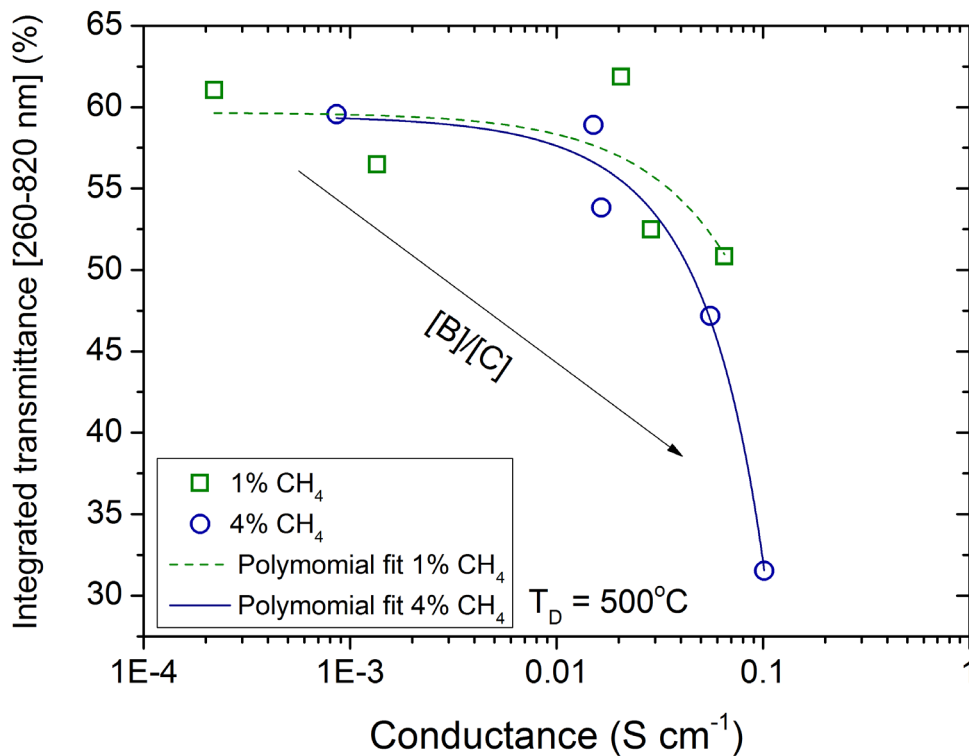

Figure 8. Dependency of transmittance on the conductivity of the BDD samples deposited on fused silica.

Next, the interpolated dependency of BDDs transmittance on conductivity is illustrated in Figure 8. It is obvious that the highly transparent BDD samples (i.e. Q_X_1) exhibit relatively low conductance. While the more conductive BDDs (i.e. Q_X_2.5 or Q_X_5) with an average transmittance of approx. 60% (integrated T ~ 55%) result in conductance of *ca.* 30 mS cm^{-1} and the resistance of *ca.* 35 Ω cm. For highly doped, highly conductive BDDs, the transmittance achieved values below 50% (integrated T ~ 40%). This phenomena is mainly driven by boron incorporation in the polycrystalline diamond structure. Increasing boron doping level causes grain re-nucleation processes, decreasing crystallite

19

sizes and produces inter-grain sp^2 rich clusters. These facts decrease transmittance and enhance conductivity, mainly inter-grain transport.

Table 3. Comparison of transparent conductive boron-doped diamond films.

Sample	Conditions T_s/CH_4	[B]/[C] [ppm]	T [%]	R_{sh} [Ohm cm]	Thickness [nm]	Substrate	Reference
Q_1_2.5	500ºC /1 %	2500	62*	48	280	f. silica	This work
Q_4_5	500ºC /4 %	5000	47*	18	530	f. silica	This work
MCD	800ºC / 0.5 %	-	25	0.026	1000	quartz	[104]
B:NCD / NCD	500ºC/ 1 %	3000	60	40	400	Corning #1737	[105]
B:NCD/AlN/ITO	700ºC / 2 %	3000	80	50-60	400	quartz	[106]
NCD BDD	700ºC / 5 %	2000	25	0.09	500	glass	[107]
LA CVD BNCD	500ºC / 4 %	15000	60-80	10-100	300	SiC, f.silica	[108]
B:NCD/AF32	600ºC / 2 %		50	500	200	AF32eco	[109]
B:NCD	700ºC / 1 %	10000	70	207	150	f. silica	[110]

* Integrated transmittance [260-820 nm] (%).

The R_{sh} and T values obtained here are enhanced compared to those reported by Granado *et al.* for thin BDD films deposited on fused silica substrates [109]. Furthermore, the above results are close to parameters reported by Taylor *et al.* for B:NCD films deposited in linear antenna CVD system. Table 3 lists the detailed comparison of transparent conductive boron-doped diamond films and its electrical as well optical parameters.

Finally, the effect of boron level at the opto-electronics properties of BDD films is not obvious. The process of film nucleation at the early stage of growth is affected by used silica

20

substrate creating specific conditions during the growth. Boron influence on parameters like the smaller crystallites size, decreased growth rate, higher sp^2 content or impurity states in band gap are in itself significant [97]. Consequently, the incorporation of defects, the concentration and coordination of the B dopants in BDD films electrode strongly modify electronic transport as well as optical properties [89]. Comparable conclusions were made by Wilson *et al.* [111], who employed conducting atomic force microscopy (C-AFM) to show that the boron uptake is non-uniform across the surface of BDD. The boron rich intergrain regions introduce impurity centres causing carrier transfer perturbations by various intragrain defects and grain boundaries.

4. Conclusion

In summary, we have investigated the electrical and optical properties of BDD films deposited at fused silica substrate in microwave plasma assisted CVD. The influence of boron doping level and methane admixture was principally studied. Raman studies reveal that as [B]/[C] ratio increases, the FWHM of diamond band get broadened up to ca. 40 cm^{-1} or 70 cm^{-1} for 1 and 4% CH_4 grown samples respectively. Since the diamond structure became more distorted, the relative sp^3/sp^2 band ratio of diamond films strongly decreased. Besides the structural studies, the deep investigation of growth kinetics, optical constants and energy band gap variations has been presented. The refractive index values ranging from 2.0 to 2.4 for BDD films deposited with low and medium boron doping level were achieved. The gap E_{gopt} significantly decreases from 3.7 eV estimated at the zero level of [B]/[C] down to 2.15 eV and 2 eV achieved for high boron levels.

Over 60% of transmittance films with resistivity as low as 48 Ω cm have been produced by suitable two-step substrate pre-treatment and PVA-DND-based seeding procedure. Consequently, there is no optimal boron doping because both R_{sh} and T physically run in the opposite direction in function of [B]/[C] increase. Such levels of opto-electronic parameters are promising for developing the integrated optical sensors, transparent electronics or optoelectrochemical biosensing devices.

technical support. The AFM measurements were done at the Faculty of Microsystems Electronics and Photonics by the courtesy of Prof. Teodor Gotszalk.

References

[1]   R. Bogdanowicz, M. Śmietana, M. Gnyba, M. Ficek, V. Straňák, Ł. Goluński, et al., Nucleation and growth of CVD diamond on fused silica optical fibres with titanium dioxide interlayer, Phys. Status Solidi A. 210 (2013) 1991–1997. doi:10.1002/pssa.201300096.

[2]   M. Smietana, J. Szmidt, M.L. Korwin-Pawlowski, W.J. Bock, J. Grabarczyk, Application of diamond-like carbon films in optical fibre sensors based on long-period gratings, Diam. Relat. Mater. 16 (2007) 1374–1377. doi:10.1016/j.diamond.2006.11.018.

[3]   A. Aleksov, M. Kubovic, N. Kaeb, U. Spitzberg, A. Bergmaier, G. Dollinger, et al., Diamond field effect transistors—concepts and challenges, Diam. Relat. Mater. 12 (2003) 391–398. doi:10.1016/S0925-9635(02)00401-6.

[4]   A.E. Fischer, Y. Show, G.M. Swain, Electrochemical Performance of Diamond Thin-Film Electrodes from Different Commercial Sources, Anal. Chem. 76 (2004) 2553–2560. doi:10.1021/ac035214o.

[5]   J. Isberg, J. Hammersberg, E. Johansson, T. Wikström, D.J. Twitchen, A.J. Whitehead, et al., High Carrier Mobility in Single-Crystal Plasma-Deposited Diamond, Science. 297 (2002) 1670–1672. doi:10.1126/science.1074374.

[6]   G.M. Swain, R. Ramesham, The electrochemical activity of boron-doped polycrystalline diamond thin film electrodes, Anal. Chem. 65 (1993) 345–351. doi:10.1021/ac00052a007.

[7]   H.B. Martin, A. Argoitia, U. Landau, A.B. Anderson, J.C. Angus, Hydrogen and Oxygen Evolution on Boron-Doped Diamond Electrodes, J. Electrochem. Soc. 143 (1996) L133–L136. doi:10.1149/1.1836901.

[8]   R. Bogdanowicz, J. Czupryniak, M. Gnyba, J. Ryl, T. Ossowski, M. Sobaszek, et al., Amperometric sensing of chemical oxygen demand at glassy carbon and silicon electrodes modified with boron-doped diamond, Sens. Actuators B Chem. 189 (2013) 30–36. doi:10.1016/j.snb.2012.12.007.

[9]   B.P. Chaplin, I. Wyle, H. Zeng, J.A. Carlisle, J. Farrell, Characterization of the performance and failure mechanisms of boron-doped ultrananocrystalline diamond

electrodes, J. Appl. Electrochem. 41 (2011) 1329–1340. doi:10.1007/s10800-011-0351-7.

[10] G.M. Swain, The Susceptibility to Surface Corrosion in Acidic Fluoride Media: A Comparison of Diamond, HOPG, and Glassy Carbon Electrodes, J. Electrochem. Soc. 141 (1994) 3382–3393. doi:10.1149/1.2059343.

[11] A. Fujishima, Diamond electrochemistry, BKC ; Elsevier, Tokyo; Amsterdam; Boston, 2005.

[12] A. Suzuki, T.A. Ivandini, K. Yoshimi, A. Fujishima, G. Oyama, T. Nakazato, et al., Fabrication, Characterization, and Application of Boron-Doped Diamond Microelectrodes for in Vivo Dopamine Detection, Anal. Chem. 79 (2007) 8608–8615. doi:10.1021/ac071519h.

[13] K. Pecková, J. Musilová, J. Barek, Boron-Doped Diamond Film Electrodes—New Tool for Voltammetric Determination of Organic Substances, Crit. Rev. Anal. Chem. 39 (2009) 148–172. doi:10.1080/10408340903011812.

[14] H. Yu, H. Wang, X. Quan, S. Chen, Y. Zhang, Amperometric determination of chemical oxygen demand using boron-doped diamond (BDD) sensor, Electrochem. Commun. 9 (2007) 2280–2285. doi:10.1016/j.elecom.2007.06.037.

[15] T.A. Ivandini, B.V. Sarada, C. Terashima, T.N. Rao, D.A. Tryk, H. Ishiguro, et al., Electrochemical detection of tricyclic antidepressant drugs by HPLC using highly boron-doped diamond electrodes, J. Electroanal. Chem. 521 (2002) 117–126. doi:10.1016/S0022-0728(02)00666-6.

[16] C. Prado, S.J. Wilkins, F. Marken, R.G. Compton, Simultaneous Electrochemical Detection and Determination of Lead and Copper at Boron-Doped Diamond Film Electrodes, Electroanalysis. 14 (2002) 262–272. doi:10.1002/1521-4109(200202).

[17] Y. Yu, Y. Zhou, L. Wu, J. Zhi, Electrochemical Biosensor Based on Boron-Doped Diamond Electrodes with Modified Surfaces, Int. J. Electrochem. Article ID 567171 (2012) doi:10.1155/2012/567171.

[18] Y.L. Zhou, R.H. Tian, J.F. Zhi, Amperometric biosensor based on tyrosinase immobilized on a boron-doped diamond electrode, Biosens. Bioelectron. 22 (2007) 822–828. doi:10.1016/j.bios.2006.03.001.

[19] C. Comninellis, Electrocatalysis in the electrochemical conversion/combustion of organic pollutants for waste water treatment, Electrochimica Acta. 39 (1994) 1857–1862. doi:10.1016/0013-4686(94)85175-1.

[20] K. Honda, M. Yoshimura, T.N. Rao, D.. Tryk, A. Fujishima, K. Yasui, et al., Electrochemical properties of Pt-modified nano-honeycomb diamond electrodes, J. Electroanal. Chem. 514 (2001) 35–50. doi:10.1016/S0022-0728(01)00614-3.

[21] E. Guinea, F. Centellas, E. Brillas, P. Cañizares, C. Sáez, M.A. Rodrigo, Electrocatalytic properties of diamond in the oxidation of a persistant pollutant, Appl. Catal. B Environ. 89 (2009) 645–650. doi:10.1016/j.apcatb.2009.01.028.

[22] A. Fabiańska, R. Bogdanowicz, P. Zięba, T. Ossowski, M. Gnyba, J. Ryl, et al., Electrochemical oxidation of sulphamerazine at boron-doped diamond electrodes: Influence of boron concentration, Phys. Status Solidi A. 210 (2013) 2040–2047. doi:10.1002/pssa.201300094.

[23] R. Bogdanowicz, A. Fabiańska, L. Golunski, M. Sobaszek, M. Gnyba, J. Ryl, et al., Influence of the boron doping level on the electrochemical oxidation of the azo dyes at Si/BDD thin film electrodes, Diam. Relat. Mater. 39 (2013) 82–88. doi:10.1016/j.diamond.2013.08.004.

[24] D. Gandini, E. Mahé, P.A. Michaud, W. Haenni, A. Perret, C. Comninellis, Oxidation of carboxylic acids at boron-doped diamond electrodes for wastewater treatment, J. Appl. Electrochem. 30 (2000) 1345–1350. doi:10.1023/A:1026526729357.

[25] K. Fabisiak, M. Szreiber, C. Uniszkiewicz, T. Runka, D. Kasprowicz, Electron paramagnetic resonance and raman spectroscopy characterization of diamond films fabricated by HF CVD method, Cryst. Res. Technol. 45 (2010) 167–172. doi:10.1002/crat.200900406.

[26] E. Brillas, C.A. Martínez-Huitle, Synthetic diamond films preparation, electrochemistry, characterization, and applications, John Wiley & Sons, Inc., Hoboken, N.J., 2011.

[27] J. Czupryniak, A. Fabiańska, P. Stepnowski, T. Ossowski, R. Bogdanowicz, M. Gnyba, et al., Application of BDD thin film electrode for electrochemical decomposition of heterogeneous aromatic compounds, Cent. Eur. J. Phys. 10 (2012) 1183–1189. doi:10.2478/s11534-012-0058-3.

[28] M. Panizza, P.A. Michaud, G. Cerisola, C. Comninellis, Electrochemical treatment of wastewaters containing organic pollutants on boron-doped diamond electrodes: Prediction of specific energy consumption and required electrode area, Electrochem. Commun. 3 (2001) 336–339. doi:10.1016/S1388-2481(01)00166-7.

[29] X.Z. Liao, R.J. Zhang, C.S. Lee, S.T. Lee, Y.W. Lam, The influence of boron doping on the structure and characteristics of diamond thin films, Diam. Relat. Mater. 6 (1997) 521–525. doi:10.1016/S0925-9635(96)00640-1.

[30] Y.-G. Lu, S. Turner, J. Verbeeck, S.D. Janssens, P. Wagner, K. Haenen, et al., Direct visualization of boron dopant distribution and coordination in individual chemical vapor deposition nanocrystalline B-doped diamond grains, Appl. Phys. Lett. 101 (2012) 041907. doi:10.1063/1.4738885.

[31] S. Gupta, A. Dudipala, O.A. Williams, K. Haenen, E. Bohannan, Ex situ variable angle spectroscopic ellipsometry studies on chemical vapor deposited boron-doped diamond films: Layered structure and modeling aspects, J. Appl. Phys. 104 (2008) 073514. doi:10.1063/1.2990058.

[32] S. Gupta, B.R. Weiner, G. Morell, Ex situ spectroscopic ellipsometry investigation of the layered structure of polycrystalline diamond thin films grown by electron cyclotron resonance-assisted chemical vapor deposition, J. Appl. Phys. 90 (2001) 1280–1285. doi:doi:10.1063/1.1384487.

[33] S. Gupta, B.R. Weiner, G. Morell, Spectroscopic ellipsometry studies of nanocrystalline carbon thin films deposited by HFCVD, Diam. Relat. Mater. 10 (2001) 1968–1972. doi:10.1016/S0925-9635(01)00387-9.

[34] Z.G. Hu, P. Prunici, P. Hess, K.H. Chen, Optical properties of nanocrystalline diamond films from mid-infrared to ultraviolet using reflectometry and ellipsometry, J. Mater. Sci. Mater. Electron. 18 (2007) 37–41. doi:10.1007/s10854-007-9175-y.

[35] A. Zimmer, O.A. Williams, K. Haenen, H. Terryn, Optical properties of heavily boron-doped nanocrystalline diamond films studied by spectroscopic ellipsometry, Appl. Phys. Lett. 93 (2008) 131910–131910–3. doi:10.1063/1.2990679.

[36] W. Gajewski, P. Achatz, O.A. Williams, K. Haenen, E. Bustarret, M. Stutzmann, et al., Electronic and optical properties of boron-doped nanocrystalline diamond films, Phys. Rev. B. 79 (2009) 045206. doi:10.1103/PhysRevB.79.045206.

[37] J. Stotter, S. Haymond, J.K. Zak, Y. Show, Z. Cvackova, G.M. Swain, Optically Transparent Diamond Electrodes for UV-Vis and IR spectroelectrochemistry, Interface. 12 (2003) 33–38.

[38] J. Stotter, J. Zak, Z. Behler, Y. Show, G.M. Swain, Optical and electrochemical properties of optically transparent, boron-doped diamond thin films deposited on quartz, Anal. Chem. 74 (2002) 5924–5930.

[39] M. Mermoux, B. Marcus, G.M. Swain, J.E. Butler, A Confocal Raman Imaging Study of an Optically Transparent Boron-Doped Diamond Electrode, J. Phys. Chem. B. 106 (2002) 10816–10827. doi:10.1021/jp0202946.

[40] Z. Remes, High optical quality nanocrystalline diamond with reduced non-diamond contamination, Diam. Relat. Mater. (2010) 453–456.

[41] A. Kromka, B. Rezek, Z. Remes, M. Michalka, M. Ledinsky, J. Zemek, et al., Formation of Continuous Nanocrystalline Diamond Layers on Glass and Silicon at Low Temperatures, Chem. Vap. Depos. 14 (2008) 181–186. doi:10.1002/cvde.200706662.

[42] S. Potocky, A. Kromka, J. Potmesil, Z. Remes, V. Vorlicek, M. Vanecek, et al., Investigation of nanocrystalline diamond films grown on silicon and glass at substrate temperature below 400 °C, Diam. Relat. Mater. 16 (2007) 744–747. doi:10.1016/j.diamond.2006.11.028.

[43] Z.G. Hu, P. Hess, Optical constants and thermo-optic coefficients of nanocrystalline diamond films at 30–500 °C, Appl. Phys. Lett. 89 (2006) 081906–081906–3. doi:doi:10.1063/1.2243863.

[44] Z.G. Hu, P. Prunici, P. Hess, K.H. Chen, Optical properties of nanocrystalline diamond films from mid-infrared to ultraviolet using reflectometry and ellipsometry, J. Mater. Sci. Mater. Electron. 18 (2007) 37–41. doi:10.1007/s10854-007-9175-y.

[45] W. Gajewski, P. Achatz, O.A. Williams, K. Haenen, E. Bustarret, M. Stutzmann, et al., Electronic and optical properties of boron-doped nanocrystalline diamond films, Phys. Rev. B. 79 (2009) 045206. doi:10.1103/PhysRevB.79.045206.

[46] D. Wu, Y.C. Ma, Z.L. Wang, Q. Luo, C.Z. Gu, N.L. Wang, et al., Optical properties of boron-doped diamond, Phys. Rev. B. 73 (2006) 012501. doi:10.1103/PhysRevB.73.012501.

[47] R. Bogdanowicz, M. Śmietana, M. Gnyba, Ł. Gołunski, J. Ryl, M. Gardas, Optical and structural properties of polycrystalline CVD diamond films grown on fused silica optical fibres pre-treated by high-power sonication seeding, Appl. Phys. A. 10.1007/s00339-014-8355-x (2014). doi:10.1007/s00339-014-8355-x.

[48] E. Scorsone, S. Saada, J.C. Arnault, P. Bergonzo, Enhanced control of diamond nanoparticle seeding using a polymer matrix, J. Appl. Phys. 106 (2009) 014908. doi:10.1063/1.3153118.

[49] R. Kiran, E. Scorsone, P. Mailley, P. Bergonzo, Quasi-Real Time Quantification of Uric Acid in Urine Using Boron Doped Diamond Microelectrode with in Situ Cleaning, Anal. Chem. 84 (2012) 10207–10213. doi:10.1021/ac301177z.

[50] R. Bogdanowicz, M. Śmietana, M. Gnyba, M. Ficek, V. Straňák, Ł. Goluński, et al., Nucleation and growth of CVD diamond on fused silica optical fibres with titanium

dioxide interlayer, Phys. Status Solidi A. 210 (2013) 1991–1997. doi:10.1002/pssa.201300096.

[51] M. Smietana, J. Szmidt, M. Dudek, P. Niedzielski, Optical properties of diamond-like cladding for optical fibres, Diam. Relat. Mater. 13 (2004) 954–957. doi:10.1016/j.diamond.2003.12.003.

[52] M. Daenen, O.A. Williams, J. D'Haen, K. Haenen, M. Nesládek, Seeding, growth and characterization of nanocrystalline diamond films on various substrates, Phys. Status Solidi A. 203 (2006) 3005–3010. doi:10.1002/pssa.200671122.

[53] J. Stotter, Y. Show, S. Wang, G. Swain, Comparison of the Electrical, Optical, and Electrochemical Properties of Diamond and Indium Tin Oxide Thin-Film Electrodes, Chem. Mater. 17 (2005) 4880–4888. doi:10.1021/cm050762z.

[54] J. Stotter, J. Zak, Z. Behler, Y. Show, G.M. Swain, Optical and Electrochemical Properties of Optically Transparent, Boron-Doped Diamond Thin Films Deposited on Quartz, Anal. Chem. 74 (2002) 5924–5930. doi:10.1021/ac0203544.

[55] R. Bogdanowicz, M. Sobaszek, J. Ryl, M. Gnyba, M. Ficek, Ł. Gołuński, et al., Improved surface coverage of an optical fibre with nanocrystalline diamond by the application of dip-coating seeding, Diam. Relat. Mater. 55 (2015) 52–63. doi:10.1016/j.diamond.2015.03.007.

[56] R. Bogdanowicz, M. Gnyba, P. Wroczyński, B.B. Kosmowski, Optoelectronic system for monitoring of thin diamond layers growth, J. Optoelectron. Adv. Mater. 12 (2010) 1660 – 1665.

[57] R. Bogdanowicz, Investigation of H2:CH4 Plasma Composition by Means of Spatially Resolved Optical Spectroscopy, Acta Phys. Pol. A. 114 (2008) A33–A38.

[58] Haldor Topsøe Semiconductor Division, Geometric factors in four point resistivity measurement., 2nd revised edition May 25, 1968, available for download from Bridge Technology website http://four-point-probes.com/haldor.html, 1968.

[59] F.M. Smits, Measurement of Sheet Resistivities with the Four-Point Probe, Bell Syst. Tech. J. 37 (1958) 711–718. doi:10.1002/j.1538-7305.1958.tb03883.x.

[60] V.V. Afanas'ev, A. Stesmans, Positive charging of thermal SiO2/(100)Si interface by hydrogen annealing, Appl. Phys. Lett. 72 (1998) 79–81. doi:10.1063/1.120650.

[61] Y. Kaibara, K. Sugata, M. Tachiki, H. Umezawa, H. Kawarada, Control wettability of the hydrogen-terminated diamond surface and the oxidized diamond surface using an atomic force microscope, Diam. Relat. Mater. 12 (2003) 560–564. doi:10.1016/S0925-9635(02)00373-4.

[62] M.N.V. Ravi Kumar, U. Bakowsky, C.M. Lehr, Preparation and characterization of cationic PLGA nanospheres as DNA carriers, Biomaterials. 25 (2004) 1771–1777. doi:10.1016/j.biomaterials.2003.08.069.

[63] A.C. Ferrari, J. Robertson, Interpretation of Raman spectra of disordered and amorphous carbon, Phys. Rev. B. 61 (2000) 14095–14107. doi:10.1103/PhysRevB.61.14095.

[64] F. Pruvost, E. Bustarret, A. Deneuville, Characteristics of homoepitaxial heavily boron-doped diamond films from their Raman spectra, Diam. Relat. Mater. 9 (2000) 295–299. doi:10.1016/S0925-9635(99)00241-1.

[65] E.A. Ekimov, V.A. Sidorov, E.D. Bauer, N.N. Mel'nik, N.J. Curro, J.D. Thompson, et al., Superconductivity in diamond, Nature. 428 (2004) 542–545. doi:10.1038/nature02449.

[66] S.J. Breuer, P.R. Briddon, \textit{Ab initio} study of substitutional boron and the boron-hydrogen complex in diamond, Phys. Rev. B. 49 (1994) 10332–10336. doi:10.1103/PhysRevB.49.10332.

[67] A.F. Azevedo, R.C. Mendes de Barros, S.H.P. Serrano, N.G. Ferreira, SEM and Raman analysis of boron-doped diamond coating on spherical textured substrates, Surf. Coat. Technol. 200 (2006) 5973–5977. doi:10.1016/j.surfcoat.2005.09.012.

[68] W.L. Wang, M.C. Polo, G. Sánchez, J. Cifre, J. Esteve, Internal stress and strain in heavily boron-doped diamond films grown by microwave plasma and hot filament chemical vapor deposition, J. Appl. Phys. 80 (1996) 1846–1850. doi:10.1063/1.362996.

[69] F. Brunet, A. Deneuville, P. Germi, M. Pernet, E. Gheeraert, J. Mambou, Effect of boron incorporation on the structure of polycrystalline diamond films, Diam. Relat. Mater. 6 (1997) 774–777. doi:10.1016/S0925-9635(96)00607-3.

[70] V.A. Krivchenko, D.V. Lopaev, P.V. Minakov, V.G. Pirogov, A.T. Rakhimov, N.V. Suetin, Study of polycrystalline boron-doped diamond films by Raman spectroscopy and optical absorption spectroscopy, Tech. Phys. 52 (2007) 1471–1474. doi:10.1134/S106378420711014X.

[71] A.C. Ferrari, S.E. Rodil, J. Robertson, Interpretation of infrared and Raman spectra of amorphous carbon nitrides, Phys. Rev. B. 67 (2003) 155306. doi:10.1103/PhysRevB.67.155306.

[72] K. Miyata, K. Kumagai, K. Nishimura, K. Kobashi, Morphology of heavily B-doped diamond films, J. Mater. Res. 8 (1993) 2845–2857. doi:10.1557/JMR.1993.2845.

[73] J. Cifre, J. Puigdollers, M.C. Polo, J. Esteve, Proceedings of the 4th European Conference on Diamond, Diamond-like and Related MaterialsTrimethylboron doping of

CVD diamond thin films, Diam. Relat. Mater. 3 (1994) 628–631. doi:10.1016/0925-9635(94)90238-0.

[74] P. Gonon, A. Deneuville, F. Fontaine, E. Gheeraert, A. Campargue, M. Chenevier, et al., Chemical vapor deposition of B-doped polycrystalline diamond films: Growth rate and incorporation efficiency of dopants, J. Appl. Phys. 78 (1995) 7404–7406. doi:10.1063/1.360393.

[75] J. Asmussen, D. Reinhard, Diamond Films Handbook, 1st edition, CRC Press, New York, 2002.

[76] R. Bogdanowicz, Characterization of Optical and Electrical Properties of Transparent Conductive Boron-Doped Diamond thin Films Grown on Fused Silica, Metrol. Meas. Syst. 21 (2014) 685–698.

[77] M. Bernard, C. Baron, A. Deneuville, About the origin of the low wave number structures of the Raman spectra of heavily boron doped diamond films, Diam. Relat. Mater. 13 (2004) 896–899. doi:10.1016/j.diamond.2003.11.082.

[78] M. Kamo, Y. Sato, S. Matsumoto, N. Setaka, Diamond synthesis from gas phase in microwave plasma, J. Cryst. Growth. 62 (1983) 642–644. doi:10.1016/0022-0248(83)90411-6.

[79] J.A. Woollam, Guide to Using WVASE32®, Wextech Systems Inc., 310 Madison Avenue, Suite 905, New York, NY 10017, 2010.

[80] H. Fujiwara, Spectroscopic Ellipsometry: Principles and Applications, Wiley-Blackwell, Chichester, England ; Hoboken, NJ, 2007.

[81] M. Gioti, D. Papadimitriou, S. Logothetidis, Optical properties and new vibrational modes in carbon films, Diam. Relat. Mater. 9 (2000) 741–745. doi:10.1016/S0925-9635(00)00244-2.

[82] M. Gioti, S. Logothetidis, Dielectric function, electronic properties and optical constants of amorphous carbon and carbon nitride films, Diam. Relat. Mater. 12 (2003) 957–962. doi:10.1016/S0925-9635(02)00222-4.

[83] G.E. Jellison Jr., V.I. Merkulov, A.A. Puretzky, D.B. Geohegan, G. Eres, D.H. Lowndes, et al., Characterization of thin-film amorphous semiconductors using spectroscopic ellipsometry, Thin Solid Films. 377–378 (2000) 68–73. doi:10.1016/S0040-6090(00)01384-5.

[84] A. Majumdar, J. Schäfer, P. Mishra, D. Ghose, J. Meichsner, R. Hippler, Chemical composition and bond structure of carbon-nitride films deposited by CH4/N2 dielectric

barrier discharge, Surf. Coat. Technol. 201 (2007) 6437–6444.
doi:10.1016/j.surfcoat.2006.12.011.

[85] H.G. Tompkins, E.A. Irene, eds., Handbook of ellipsometry, William Andrew Pub. ;
Springer, Norwich, NY : Heidelberg, Germany, 2005.

[86] S. Gupta, B.R. Weiner, G. Morell, Ex situ spectroscopic ellipsometry investigation of the
layered structure of polycrystalline diamond thin films grown by electron cyclotron
resonance-assisted chemical vapor deposition, J. Appl. Phys. 90 (2001) 1280–1285.
doi:doi:10.1063/1.1384487.

[87] J. Robertson, Diamond-like amorphous carbon, Mater. Sci. Eng. R Rep. 37 (2002) 129–
281. doi:10.1016/S0927-796X(02)00005-0.

[88] G. Davies, Properties and growth of diamond, INSPEC, the Institution of Electrical
Engineers, 1994.

[89] M. Sobaszek, Ł. Skowroński, R. Bogdanowicz, K. Siuzdak, A. Cirocka, P. Zięba, et al.,
Optical and electrical properties of ultrathin transparent nanocrystalline boron-doped
diamond electrodes, Opt. Mater. 42 (2015) 24–34. doi:10.1016/j.optmat.2014.12.014.

[90] J. Nakamura, E. Kabasawa, N. Yamada, Y. Einaga, D. Saito, H. Isshiki, et al., Electronic
structures of B2p and C2p levels in boron-doped diamond films studied using soft x-ray
absorption and emission spectroscopy, Phys. Rev. B. 70 (2004) 245111.
doi:10.1103/PhysRevB.70.245111.

[91] F.J. Arregui, Sensors Based on Nanostructured Materials, Springer, 2010.

[92] P.W. May, W.J. Ludlow, M. Hannaway, P.J. Heard, J.A. Smith, K.N. Rosser, Raman
and conductivity studies of boron-doped microcrystalline diamond, facetted
nanocrystalline diamond and cauliflower diamond films, Diam. Relat. Mater. 17 (2008)
105–117. doi:10.1016/j.diamond.2007.11.005.

[93] A. Lewkowicz, A. Synak, B. Grobelna, P. Bojarski, R. Bogdanowicz, J. Karczewski, et
al., Thickness and structure change of titanium(IV) oxide thin films synthesized by the
sol–gel spin coating method, Opt. Mater. 36 (2014) 1739–1744.
doi:10.1016/j.optmat.2014.02.033.

[94] H. Lee, I.-Y. Kim, S.-S. Han, B.-S. Bae, M.K. Choi, I.-S. Yang, Spectroscopic
ellipsometry and Raman study of fluorinated nanocrystalline carbon thin films, J. Appl.
Phys. 90 (2001) 813–818. doi:10.1063/1.1378337.

[95] A. Taylor, L. Fekete, P. Hubík, A. Jäger, P. Janíček, V. Mortet, et al., Large area
deposition of boron doped nano-crystalline diamond films at low temperatures using

microwave plasma enhanced chemical vapour deposition with linear antenna delivery, Diam. Relat. Mater. 47 (2014) 27–34. doi:10.1016/j.diamond.2014.05.002.

[96] J.-P. Lagrange, A. Deneuville, E. Gheeraert, A large range of boron doping with low compensation ratio for homoepitaxial diamond films, Carbon. 37 (1999) 807–810. doi:10.1016/S0008-6223(98)00275-9.

[97] P. Azadfar, M. Ghoranneviss, S.M. Elahi, N. Farhadyar, A. Salar Elahi, Growth of boron-doped diamond nanoclusters using the HFCVD technique, J. Cryst. Growth. 415 (2015) 166–169. doi:10.1016/j.jcrysgro.2015.01.001.

[98] M. Sobaszek, K. Siuzdak, M. Sawczak, J. Ryl, R. Bogdanowicz, Fabrication and characterization of composite TiO2 nanotubes/boron-doped diamond electrodes towards enhanced supercapacitors, Thin Solid Films. (n.d.). doi:10.1016/j.tsf.2015.09.073.

[99] V.P. Godbole, G.S. Kim, M.A. Dar, Y.S. Kim, H.K. Seo, G. Khang, et al., Hot filament chemical vapour deposition processing of titanate nanotube coatings, Nanotechnology. 16 (2005) 1186. doi:10.1088/0957-4484/16/8/035.

[100] M. Tsigkourakos, T. Hantschel, Z. Xu, B. Douhard, J. Meersschaut, Y. Zou, et al., Suppression of boron incorporation at the early growth phases of boron-doped diamond thin films, Phys. Status Solidi A. 212 (2015) 2595–2599. doi:10.1002/pssa.201532185.

[101] M. Werner, R. Job, A. Zaitzev, W.R. Fahrner, W. Seifert, C. Johnston, et al., The Relationship between Resistivity and Boron Doping Concentration of Single and Polycrystalline Diamond, Phys. Status Solidi A. 154 (1996) 385–393. doi:10.1002/pssa.2211540127.

[102] J. Barjon, N. Habka, C. Mer, F. Jomard, J. Chevallier, P. Bergonzo, Resistivity of boron doped diamond, Phys. Status Solidi RRL – Rapid Res. Lett. 3 (2009) 202–204. doi:10.1002/pssr.200903097.

[103] M. Tsigkourakos, T. Hantschel, D.K. Simon, T. Nuytten, A.S. Verhulst, B. Douhard, et al., On the local conductivity of individual diamond seeds and their impact on the interfacial resistance of boron-doped diamond films, Carbon. 79 (2014) 103–112. doi:10.1016/j.carbon.2014.07.048.

[104] J. Stotter, J. Zak, Z. Behler, Y. Show, G.M. Swain, Optical and electrochemical properties of optically transparent, boron-doped diamond thin films deposited on quartz, Anal. Chem. 74 (2002) 5924–5930.

[105] O.A. Williams, M. Nesládek, Growth and properties of nanocrystalline diamond films, Phys. Status Solidi A. 203 (2006) 3375–3386. doi:10.1002/pssa.200671406.

[106] V. Zuerbig, W. Pletschen, J. Hees, R.E. Sah, L. Kirste, N. Heidrich, et al., Transparent diamond electrodes for tunable micro-optical devices, Diam. Relat. Mater. 38 (2013) 101–103. doi:10.1016/j.diamond.2013.06.010.

[107] A. Kovalenko, P. Ashcheulov, A. Guerrero, P. Heinrichová, L. Fekete, M. Vala, et al., Diamond-based electrodes for organic photovoltaic devices, Sol. Energy Mater. Sol. Cells. 134 (2015) 73–79. doi:10.1016/j.solmat.2014.11.035.

[108] A. Taylor, P. Ashcheulov, M. Čada, L. Fekete, P. Hubík, L. Klimša, et al., Effect of plasma composition on nanocrystalline diamond layers deposited by a microwave linear antenna plasma-enhanced chemical vapour deposition system, Phys. Status Solidi A. 212 (2015) 2418–2423. doi:10.1002/pssa.201532183.

[109] T.C. Granado, G. Neusser, C. Kranz, J.B.D. Filho, V. Carabelli, E. Carbone, et al., Progress in transparent diamond microelectrode arrays, Phys. Status Solidi A. 212 (2015) 2445–2453. doi:10.1002/pssa.201532168.

[110] W.S. Yeap, D. Bevk, X. Liu, H. Krysova, A. Pasquarelli, D. Vanderzande, et al., Diamond functionalization with light-harvesting molecular wires: improved surface coverage by optimized Suzuki cross-coupling conditions, RSC Adv. 4 (2014) 42044–42053. doi:10.1039/C4RA04740K.

[111] N.R. Wilson, S.L. Clewes, M.E. Newton, P.R. Unwin, J.V. Macpherson, Impact of Grain-Dependent Boron Uptake on the Electrochemical and Electrical Properties of Polycrystalline Boron Doped Diamond Electrodes, J. Phys. Chem. B. 110 (2006) 5639–5646. doi:10.1021/jp0547616.

Figure captions:

Figure 1. Wetting properties of fused silica substrate before and after hydrogenation treatment.

Figure 2. Raman spectra of boron-doped diamond films ([B]/[C]=0; 1000; 2,500; 5000; 10000 ppm) deposited at fused silica in temperature of 500°C vs. two different methane concentrations (1% and 4%) in gas mixture.

Figure 3. Thickness and surface roughness (SRL) of the BDD samples deposited on the fused silica estimated by stylus profilometer and spectroscopic ellipsometry. Growth rates of BDD films are placed in plot for comparison of time kinetics. Insets: SEM micro-images of BDD surface (3 x 2 μm) taken with magnification of 10 000 x.

Figure 4. Variation of optical constant for boron-doped diamond films obtained on quartz slides at various boron doping level and methane admixture.

Figure 5. Transmittance of BDD films deposited at fused silica substrates vs various boron doping and methane admixture.

Figure 6. Refractive index recorded at 550 nm and in-direct optical band gaps of BDD samples with increasing boron concentrations and various methane admixture.

Figure 7. Surface resistivity of BDD films vs various boron doping level and methane admixture in the plasma. The BDDs deposited on fused silica and silicon wafer covered by thick SiO_2 have been presented for comparison.

Figure 8. Dependency of transmittance on the conductivity of the BDD samples deposited on fused silica.